PERGAMON

Materials Science in Semiconductor Processing 2 (1999) 271–279

MATERIALS SCIENCE IN SEMICONDUCTOR PROCESSING

Two-dimensional plasma reactor simulation with self-consistent coupling of gas flow with plasma transport

Sang Ki Nam[a], Chee Burm Shin[a], Demetre J. Economou[b,*]

[a]*Department of Chemical Engineering, Ajou University, Suwon, 442-749, South Korea*
[b]*Plasma Processing Laboratory, Department of Chemical Engineering, University of Houston, Houston, TX 77204-4792, USA*

Abstract

A two-dimensional (2-D) fluid simulation applicable to high density plasma reactors was developed which couples gas flow with plasma transport in a self-consistent manner. Modified boundary conditions were used at the reactor walls to accommodate transport at low pressures. A modular approach circumvented the disparity in time scales and a quasi-neutral plasma assumption overcame the disparity in length scales. This approach allowed for a simulation tool that can execute rapidly on a desktop computer, and is, therefore, suitable for Technology Computer-Aided Design (TCAD). Simulation results for an electron cyclotron resonance (ECR) plasma system showed good agreement with experimental data on electron density and temperature as a function of plasma power and pressure. Also, the gas pressure drop in the reactor was predicted correctly by the simulation. Further simulation studies showed the effect of power and pressure on ion flux uniformity on a wafer substrate.

1. Introduction

High density plasma (HDP) reactors [1] are widely accepted for manufacturing microelectronic circuits with sub-0.25 μ linewidths. Major advantages of HDP tools compared to more traditional plasma reactors are: (a) lower pressure operation which may promote plasma uniformity over large diameter wafers and more directional ion bombardment of the wafer surface; and (b) independent control of plasma density and ion bombardment energy by decoupling plasma production from the substrate biasing circuit. HDP tools include inductively coupled plasma (ICP), electron cyclotron resonance (ECR), helicon, and helical resonator reactors.

Modeling and simulation can provide insight into the spatiotemporal plasma flow, and can aid in the design of new plasma sources [1,2]. Most plasma simulations reported thus far do not consider the coupled effects of gas flow with plasma transport [3–8] or account for gas flow in a decoupled (non self-consistent) manner [9,10]. A stationary background gas [3–7] or purely diffuse flow of gases (no convection) [8] is assumed. Gas flow can affect plasma reactor characteristics, especially near the inlet and pumping ports where convective gas velocities are higher and the so-called Peclet number ($Pe = uL/D$) exceeds unity. Here u is the convective flow velocity, L is a characteristic length scale and D is the species diffusivity. The Peclet number shows the relative importance of convection compared to diffusion in controlling species transport. Two-dimensional plasma simulation including gas flow effects have been reported [11,12] in the literature. Although the computational time was not reported, these simulations are expected to be comparatively

* Corresponding author.

1369-8001/99/$ - see front matter
PII: S1369-8001(99)00015-3

slow since the Poisson equation is used. Using the quasineutral approximation provides a tremendous computational advantage since the very short time scales of charge equilibration are bypassed. Meyyappan and Govindan have used the quasi-neutral plasma approximation to study plasma transport in a one-dimensional (1-D) model system including gas flow in a self-consistent manner [13]. The same approach was extended to a 2-D ICP source [14]. We have used the quasi-neutral plasma approximation before to simulate 2-D [8,15,31] and 3-D [16] high density plasmas using the diffusive gas transport assumption ($Pe < 1$).

In this paper we report on a rapid 2-D self-consistent high density plasma reactor simulation using the fluid approximation. The boundary conditions are modified to accommodate transport at reduced pressures. The simulation is validated by comparing predictions of gas pressure drop, electron density and electron temperature with experimental data taken in an ECR reactor [17]. Previous simulations of ECR reactors have been reported in [3,13,18–22].

To be used as a TCAD tool, a computer simulation must be accurate, user friendly and able to execute rapidly on a desktop computer. These features allow one to conduct parametric investigations easily to study the effect of different reactor designs and operating conditions on the plasma etch or deposition characteristics.

2. Model formulation

The present model employs a 'modular' approach similar to that reported earlier [23]. However, a Navier–Stokes gas flow module is implemented instead of purely diffusive gas transport. Also, the spatial profile of power deposited into the plasma is assumed instead of calculated by an electromagnetics module. The power deposition is used in an electron energy module to determine the electron temperature and the rate coefficients of electron-impact reactions. These are in turn used as source terms in separate modules describing neutral and charged species transport. By iterating among the modules, a self-consistent solution is obtained. This modular approach is in essence an 'equation splitting' strategy that is used to overcome the disparate time scales associated with electron (< 1 ns) and heavy species (tens of μs for ions and perhaps hundreds of ms or longer for neutrals) transport and chemistry. Furthermore, the computation time is shorter as the bandwidth of the matrices resulting after spatial discretization is reduced greatly by implementing a smaller number of equations per module.

A number of simplifications have been introduced to streamline the computation. These simplifications are also used in the Molecular Plasma Reactor Simulator (MPRES) [8,15].

1. The reactor is separated into bulk plasma and sheath to remove the extreme spatial stiffness due to the thin sheaths. For the high plasma density (10^{11}–10^{12} cm^{-3}) of interest here, the sheath thickness is of the order of hundreds of μm. In contrast, the reactor typically has dimensions of tens of cm. The high degree of spatial stiffness ($O(10^3)$) requires a large number of carefully designed elements to obtain the solution. In order to allow rapid, widely convergent solutions, the sheath has been separated out of the bulk plasma simulation. This is feasible for the high density plasma by taking advantage of the thin sheaths, which can be assumed collisionless. At 10 mtorr, the ion mean free path is of the order of 0.5 cm, about an order of magnitude greater than the sheath thickness. For collisionless sheaths the Bohm criterion is applied for flux of positively charged species. In order to be consistent with the Bohm criterion for ions, the sheath edge is defined as the point where the ions have been accelerated to the Bohm velocity, i.e. the pre-sheath is included as part of the bulk plasma. Negatively charged ionic species are given a negligible density at the sheath edge. This is a good assumption for not strongly electronegative plasmas as the pre-sheath fields will prevent negative ions from reaching the sheath edge.
2. Quasineutrality is used to calculate the electron density:

$$n_e = \frac{1}{e}\sum_i z_i n_i \tag{1}$$

where z_i is the charge on ion i, and n_e and n_i are the electron and ion (positive and/or negative) densities, respectively, and e is the elementary charge. This is an excellent assumption for the conditions studied, since the Debye length is exceedingly short compared to the reactor dimensions. Use of Eq. (1) instead of the Poisson equation makes the system of equations describing the plasma reactor similar to that for neutral flow (e.g., CVD) reactors which is inherently simpler to solve.
3. In order to calculate the space charge fields (which would have been calculated by the Poisson equation), the electrons are assumed to be in Boltzmann equilibrium [1, p. 40]. This means that the space charge field $\boldsymbol{E}_s$ counterbalances the electron pressure, $p_e = n_e k T_e$:

$$\boldsymbol{E}_s = -\frac{\nabla(n_e k T_e)}{e n_e} \tag{2}$$

where k and T_e are the Boltzmann constant and electron temperature, respectively. Ions are accelerated by this space charge field. The use of electron

temperature T_e implicitly assumes that the electron energy distribution function (EEDF) is Maxwellian. However, MPRES can make use of non-Maxwellian EEDFs. In such cases, T_e is defined as two thirds of the average electron energy.

4. The mixture of feed gas and generated species is treated as a continuum. To justify the use of a continuum approach at low pressures, modifications to the boundary conditions for gas flow and heat transfer are required [2].
5. The ideal gas law and Newton's law of viscosity apply.
6. Multicomponent transport [13,14] is not considered. This is expected to be accurate for 'dilute' mixtures.

Implementing the above simplifications results in a dramatic reduction in the CPU time required to achieve a converged solution. This makes the simulation particularly attractive for TCAD applications. An electropositive (argon) plasma is considered below which contains electrons, positive ions, and one (lumped) metastable species in a sea of ground state neutral atoms.

The conservation equations of mass, momentum and energy for the neutral gas are

$$\frac{D\rho}{Dt} = -\rho(\nabla \cdot \mathbf{v}) \tag{3}$$

$$\rho\frac{D\mathbf{v}}{Dt} = -\nabla p + \rho\mathbf{g} + \nabla \cdot \tau \tag{4}$$

$$\rho C_p\frac{DT}{Dt} = \frac{Dp}{Dt} + \nabla \cdot (K\nabla T) + \tau: (\nabla\mathbf{v}) + \rho(\mathbf{v} \cdot \mathbf{g}) + Q_{coll} \tag{5}$$

where ρ is gas density; $\mathbf{v}$ is gas velocity; τ is stress tensor; p is pressure; $\mathbf{g}$ is gravitational acceleration; K is gas thermal conductivity; and Q_{coll} is the energy gain of the neutral gas due to its interaction with the charged particles. This term was taken to be 5% of the power deposited in the plasma.

The conservation equations for positive ions and metastable atoms are

$$\frac{\partial n_+}{\partial t} + \nabla \cdot \boldsymbol{J}_+ = \sum_j R_{+j} \tag{6}$$

$$\frac{\partial n_*}{\partial t} + \nabla \cdot \boldsymbol{J}_* = \sum_j R_{*j} \tag{7}$$

Due to the electroneutrality, the electron density in the bulk plasma is given by

$$n_e = n_+ \tag{8}$$

Table 1
Boundary conditions

v	$v \cdot s = \lambda(\partial v_s/\partial n)$
T	$T - T_w = (2/P_r)[(2-A)/A][\gamma/(\gamma+1)](\partial T/\partial n)$
n_+	$J_+ = n_+ u_B$
n_*	$n_* = 0$
T_e	$q_e = (\frac{5}{2}kT_e)\frac{1}{4}\sqrt{(8kT_e/\pi m_e)}n_e$

The particle fluxes are

$$\boldsymbol{J}_+ = -D_+\nabla n_+ + \mu_+ n_+ \boldsymbol{E}_s + n_+\mathbf{v} \tag{9}$$

$$\boldsymbol{J}_* = -D_*\nabla n_* + n_*\mathbf{v} \tag{10}$$

In the above equations, n_j, $\boldsymbol{J}_j$, D_j, and μ_j are particle density, flux, diffusivity, and mobility, respectively. Subscripts + and * denote positive ions and metastable atoms, respectively. The summation on the right-hand-side of Eqs. (6) and (7) is overall homogeneous reactions creating and destroying the corresponding particle. The reactions considered are listed in [24] which also gives the rate coefficients as a function of electron energy.

The electron energy balance reads

$$\frac{\partial}{\partial t}\left(\frac{3}{2}n_e kT_e\right) + \nabla \cdot \boldsymbol{q}_e + e\boldsymbol{J}_e \cdot \boldsymbol{E} + P_{coll} - P_{ext} = 0 \tag{11}$$

with the total electron energy flux is given by

$$\boldsymbol{q}_e = -K_e\nabla T_e + \tfrac{5}{2}kT_e J_e \tag{12}$$

where the thermal conductivity of electrons is given by $K_e = 3/2kD_e n_e$. P_{coll} is the electron energy lost through collisions and P_{ext} is the external power coupled to the plasma. In the present work, P_{ext} was assumed to have a power profile analogous to that of Ref. [3].

Boundary conditions (shown in Table 1) are imposed essentially at the reactor wall assuming a very thin sheath. The sheath is, therefore, handled as a discontinuity of the potential at the wall. The positive ion flux out of the plasma is set equal to the local ion density times the local Bohm velocity. The negative ion density is set equal to zero at the walls. This is valid for continuous wave plasmas for which the negative ions are confined by the electrostatic fields. The gas velocity perpendicular to the wall is set equal to zero. At the reactor entrance, a uniform gas velocity profile is used (plug flow). At the reactor exit, a zero traction boundary condition is applied. Symmetry is imposed on axis. Finally, the wall temperature is specified at 298 K. Multicomponent/multitemperature effects were not included in the simulation. For example, pressure

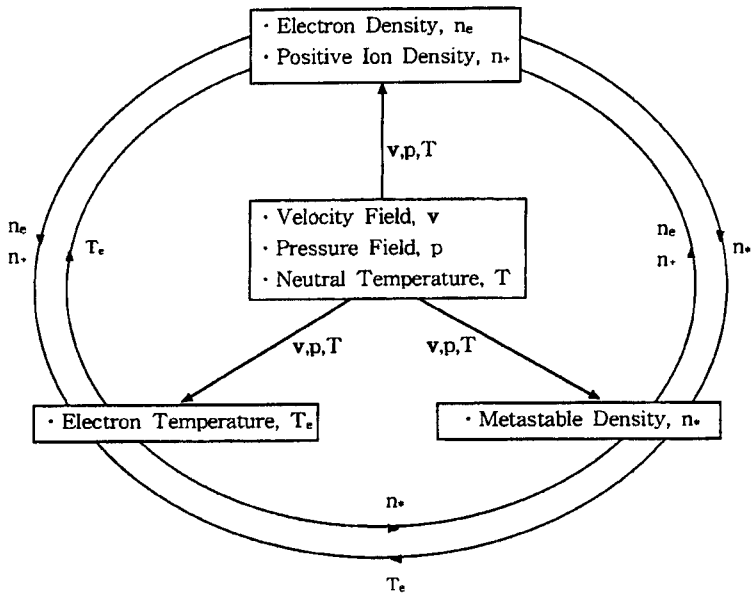

Fig. 1. Schematic of the modular approach used to achieve fast convergence to the steady-state solution.

p does not include the electron pressure (see Ref. [13]). This makes the simulation much faster, but also limits the range of applicability of the model. It should be mentioned, however, that the pressure one measures with a pressure transducer does not include electrons (they will recombine!). In that sense, the calculated pressure (w/o electron pressure) is more directly comparable to the measured pressure.

3. Method of solution

The governing Eqns. (3)–(7) and (11) subject to the corresponding boundary conditions were solved numerically by using the Galerkin finite element method [25]. The computational domain (corresponding to the reactor shown later in Fig. 3) was divided into a mesh consisting of 219 biquadratic elements and 957 nodes. On this mesh, the unknown variables were approximated by piecewise continuous polynomials of Lagrange type. The choice of interpolation functions used for gas pressure p is constrained, because the weak form of Eqs. (3) and (4) contains the first derivatives of velocities and no derivatives of pressure. In addition, the essential boundary conditions of the formulation do not include specification of pressure; p enters as a natural boundary condition. This implies that pressure need not be carried as a variable that is continuous across interelement boundaries. These observations lead to the conclusion that the pressure variable should be interpolated with functions that are one order less than those used for the velocity field. Thus, biquadratic interpolation of the neutral gas velocities, neutral gas temperature, species densities, and electron temperature was adopted, while bilinear interpolation was used for pressure. Equal interpolation of the velocities and pressure is known to give inaccurate results [26,27]. The gas density was obtained based on the ideal gas law, i.e. the gas density was treated as a function of neutral gas pressure and temperature. Spatial discretization resulted in a set of coupled nonlinear algebraic equations.

In order to reduce the computational load, a modular approach was followed as before [23]. The modules

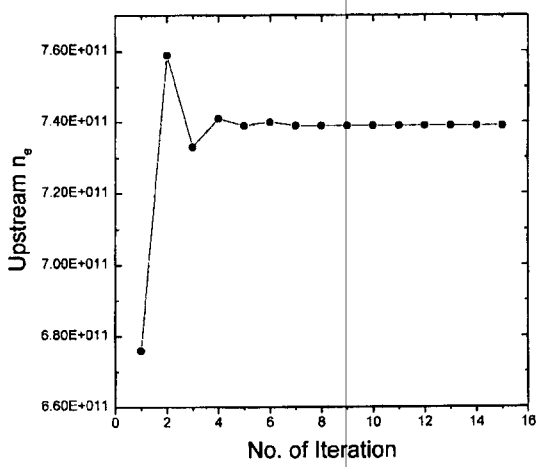

Fig. 2. Convergence of the upstream electron density vs number of iterations through the electron density module.

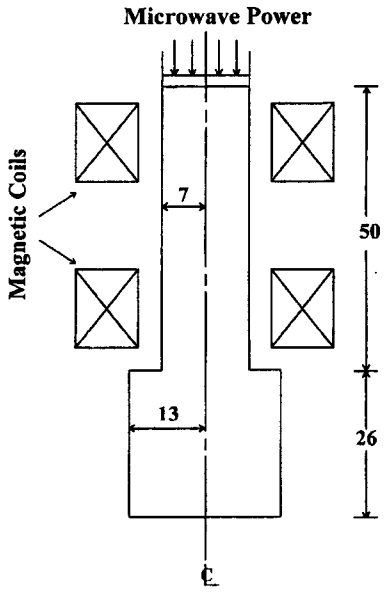

Fig. 3. Schematic diagram of the ECR reactor used for computation. Dimensions are in cm.

used in the present work are shown in Fig. 1. Different modules were used for the neutral gas velocity, neutral gas pressure, and neutral gas temperature, species density, and electron temperature. Necessary information was cycled back-and-forth among the modules until convergence. A converged solution was normally achieved after seven to eight iterations through each particular module (see Fig. 2). Calculations were performed on a Sun Ultra 140 workstation. The CPU time required to achieve a convergence among all modules was about 10 min for the set of geometrical and operating conditions given below. Initial densities and temperatures may be estimated by using a zero-dimensional (global) model of the discharge [1].

4. Results and discussion

The model developed above does not account for magnetic field effects. However, as a first attempt, we compare the model predictions with experimental data from an ECR system; a similar approach was followed in [13]. We note that, in a steady-state low pressure

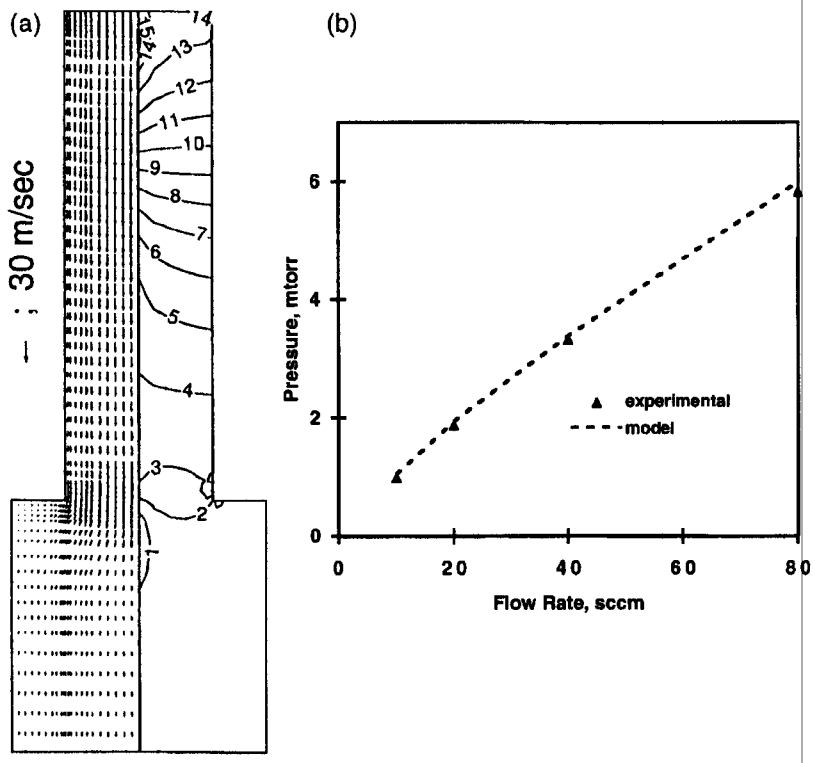

Fig. 4. (a) Gas flow velocity vectors (left) and neutral gas pressure (right) for the base case conditions. Contour numbers of 1 and 15 correspond to 2.64 and 3.84 dynes/cm^2, respectively. Linear interpolation applies in-between. (b) Comparison of model predictions (line) with experimental data from Ref. [17] (points) of upstream chamber pressure in the absence of plasma.

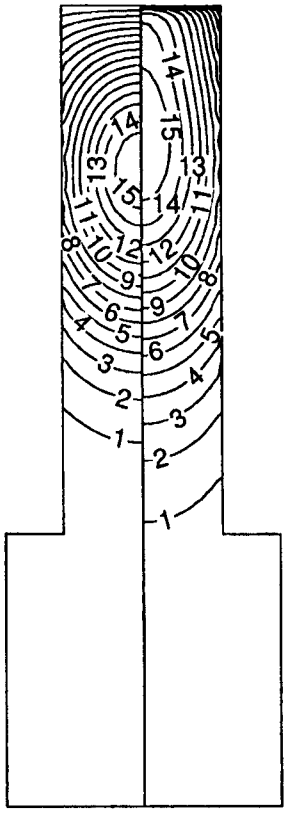

Fig. 5. Neutral gas temperature (left) and electron temperature (right) for the base case conditions. For the left side, contour numbers of 1 and 15 correspond to 323 and 671 K, respectively. For the right side, contour numbers of 1 and 15 correspond to 2.9 and 6.6 eV, respectively. For both sides, linear interpolation applies in-between.

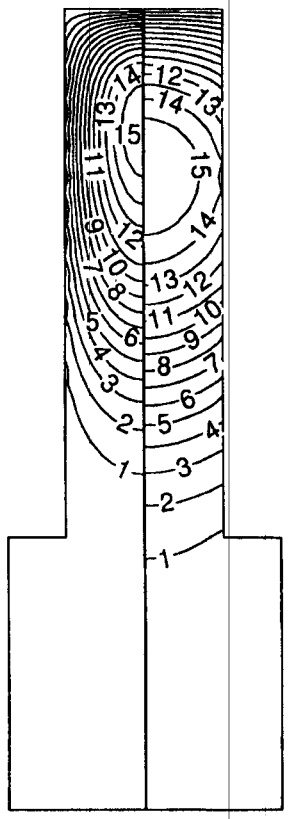

Fig. 6. Metastable species density (left) and electron density (right) for the base case conditions. For the left side, contour numbers of 1 and 15 correspond to 7.54×10^{10} and 1.13×10^{12} cm^{-3}, respectively. For the right side, contour numbers of 1 and 15 correspond to 4.65×10^{10} and 6.98×10^{11} cm^{-3}, respectively. For both sides, linear interpolation applies in-between.

electropositive plasma, the electron density is controlled by ion losses to the wall, and ions are only weakly magnetized. Also, to a first approximation, the electron temperature is a function of geometry, pressure and the type of gas. Hence, it is not surprising that the predictions of electron density and temperature are quite reasonable (see below). In addition, the neutral gas flow is not affected by the magnetic field and thus, comparison of predictions of gas pressure drop with experimental data should be valid, even for a magnetized system as an ECR source. This assumes that the degree of ionization is less than about 10%.

A schematic of the ECR system used to compare model predictions with experimental data is shown in Fig. 3. This system is similar to that used for ECR diagnostics by Gorbatkin et al. [17]. The following operating conditions were chosen as base case: downstream pressure 2 mtorr, plasma power 500 W, and flow rate 5 sccm of pure argon. In discussing the figures below, the base case values were used unless noted otherwise.

The gas velocity vector plot is shown in Fig. 4 (left-hand-side). The effects of convection due to gas flow and the rarefaction of neutral density due to gas heating were considered in the simulation. These effects have been largely neglected in previous fluid simulation. The gas velocity is appreciable even near the walls due to 'slip'. The velocity decreases in the downstream chamber as the cross sectional area available for flow increases. There is evidence of gas acceleration as the flow passes through the power deposition zone where the gas is heated. The calculated pressure drop through the system agrees well with the measurements of Gorbatkin et al. [17]. For example, for 5 sccm flow, the measured gas pressure at the downstream location was 75% of that at the resonance zone. The simulation predicted a fraction of 72%, in close agreement with

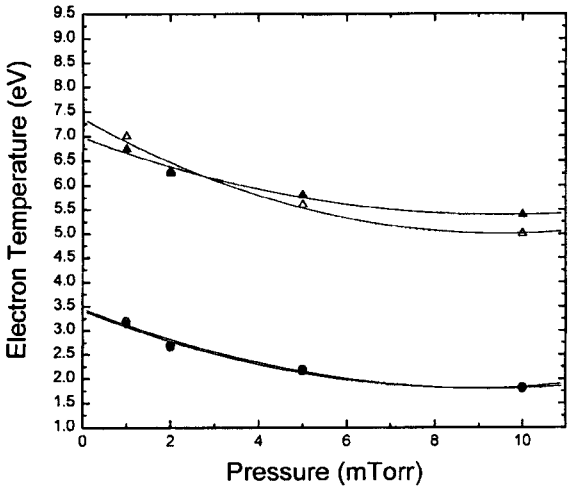

Fig. 7. Comparison between experimental data (open symbols) and simulation results (solid symbols) for the pressure dependence of the electron temperature upstream (triangles) and downstream (circles).

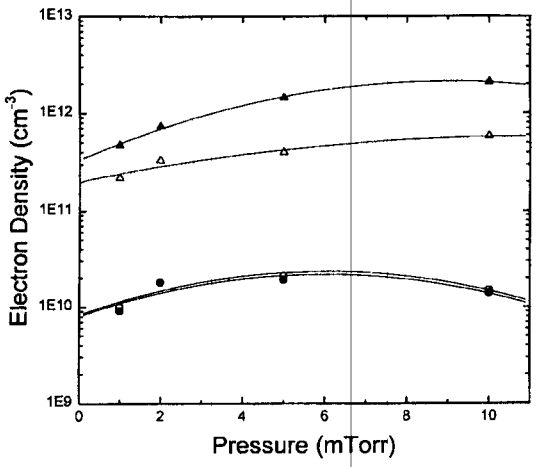

Fig. 8. Comparison between experimental data (open symbols) and simulation results (solid symbols) for the pressure dependence of the electron density upstream (triangles) and downstream (circles).

the measurement. Further comparison between measured and calculated pressures (without a plasma in the chamber), is shown in Fig. 4(b). A 1-D simulation [13] can also capture the correct value of the pressure drop, through appropriate averaging of the equations.

Fig. 5 illustrates the distributions of neutral gas temperature (left) and electron temperature (right). Gas heating is mainly due to charge exchange collisions with ions and ion–electron recombination with minor contribution from elastic collisions. The same conclusion was reached by Govindan et al. [13]. The maximum in neutral gas temperature is located in the high plasma density region in the power deposition zone. The neutral temperature peaks on the axis of the ECR chamber and decreases in the radial direction due to heat losses to the ambient through the walls. Measurements of gas temperature in ECR systems under comparable conditions [28–30] show similar values with those predicted by the simulation. The electron temperature also reaches a maximum in the power deposition zone. Due to the high conductivity of electrons at low pressure, the electron temperature remains relatively high even in the downstream chamber.

Fig. 6 shows the distribution of argon metastable density (left) and electron density (right). Metastables are destroyed at the walls and their density in the downstream chamber is two orders of magnitude lower than the peak value. The electron density peaks in the power deposition region. Significant density gradients exist in both the radial and axial directions and the density in the source chamber is higher than that in the downstream chamber by an order of magnitude.

In Fig. 7, the calculated electron temperature at various pressures is compared with the Langmuir probe data of Gorbatkin et al. [17]. The experimental measurements were made on-axis in the source chamber (19 cm from the top of the reactor) and in the downstream chamber (62 cm from the top of the reactor). In both locations, the electron temperature drops with increasing pressure, as expected. The agree-

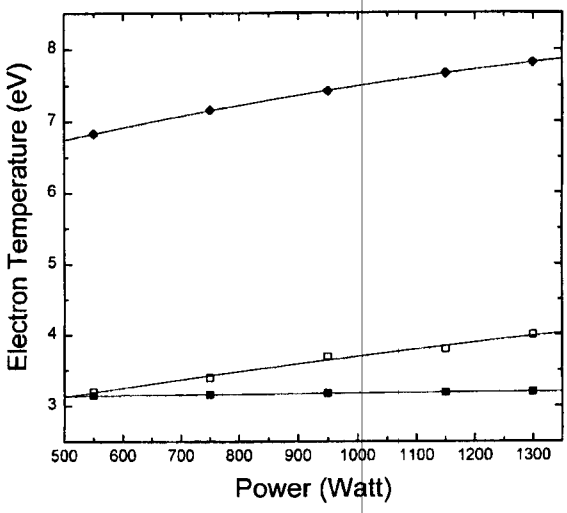

Fig. 9. Comparison between experimental data (open symbols) and simulation results (solid symbols) for the power dependence of the electron temperature upstream (diamonds) and downstream (squares).

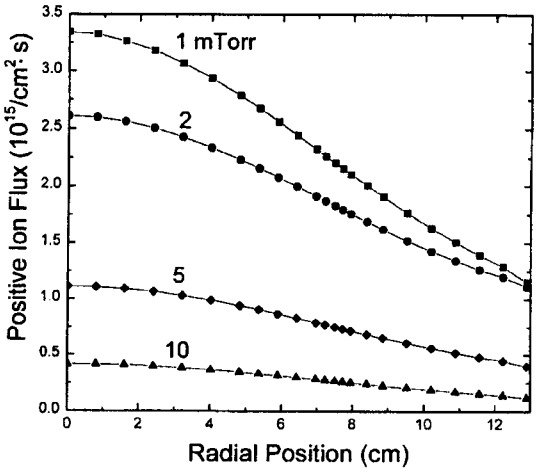

Fig. 10. Predicted ion flux uniformity on a 26 cm diameter substrate placed at the mid-axial position of the downstream chamber vs pressure.

ment between calculation and experiment is good in both the source and downstream chambers.

In Fig. 8, predictions of electron density at various pressures are compared with experimental data of Gorbatkin et al. [17]. The predicted values in the source chamber are about two to four times higher than those of the experiment, while the predicted values in the downstream chamber are close to the experimental data. Langmuir probe measurements in magnetized plasmas are quite difficult. Gorbatkin et al. expect an uncertainty of a few times [17], placing the predictions in reasonable agreement with the data. Furthermore, the general trends of the variation of predicted electron density appear to be in good agreement with those of the experimental data.

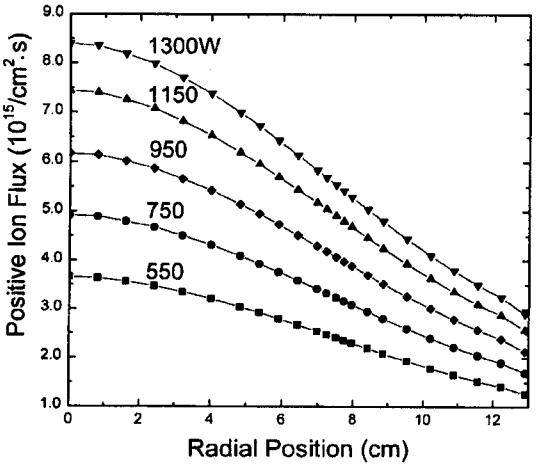

Fig. 11. Predicted ion flux uniformity on a 26 cm diameter substrate placed at the mid-axial position of the downstream chamber vs power.

Table 2
Uniformity Index vs pressure and power

	UI
Pressure (mtorr)	
1	0.55
2	0.45
5	0.53
10	0.64
Power (W)	
550	0.55
750	0.55
950	0.55
1150	0.55
1300	0.55

Fig. 9 shows the comparison between predictions and experiment on the variation of electron temperature at 1 mtorr as a function of plasma power. Again, the predictions are in reasonable agreement with the data (there were no measurements of electron temperature versus power at the upstream chamber).

Finally, Figs. 10 and 11 show the predicted ion flux radial uniformity at the (axial) mid-plane of the downstream chamber for different pressures and powers, respectively. The corresponding uniformity index is shown in Table 2. The uniformity index (UI) is defined as

$$UI = (\max - \min)/(2 \times \text{avg})$$

where max, min, and avg are the maximum, minimum, and average values of the flux, respectively. UI is independent of power and is generally decreasing (better uniformity) with decreasing pressure.

5. Conclusions

A 2-D fluid simulation applicable to high density plasma reactors was developed which couples gas flow with plasma transport in a self-consistent manner. A Navier–Stokes equation module and a neutral gas energy balance provided the neutral fluid velocity, pressure and temperature distributions in the reactor. Modified boundary conditions were used at the reactor walls to accommodate transport at low pressures. A modular approach circumvented the disparity in time scales and a quasi-neutral plasma assumption overcame the disparity in length scales. This approach allowed for a simulation tool that can execute rapidly (~10 min for an argon plasma) on a desktop computer, and is, therefore, suitable for TCAD. Simulation

results for an ECR plasma system showed good agreement with experimental data on electron density and temperature as a function of plasma power and pressure. Also, the gas pressure drop in the reactor was predicted correctly by the simulation. Further simulation studies showed the effect of power and pressure on ion flux uniformity in the downstream chamber. Uniformity was predicted to be almost independent of power, while decreasing pressure resulted in generally better uniformity.

Acknowledgements

D. J. Economou acknowledges the National Science Foundation (CTS-9713262) for providing partial financial support for this project.

References

[1] Leiberman MA, Lichtenberg AJ. Principles of Plasma Discharges and Materials Processing. New York: John Wiley and Sons, 1994.
[2] Meyyappan M. In: Mayyappan M, editor. Computational Modeling in Semiconductor Processing. Boston: Artech House, 1995 Chapter 5.
[3] Porteous RK, Wu HM, Graves DB. Plasma Sources Sci Technol 1994;3:25.
[4] Lymberopoulos DP, Economou DJ. J Vac Sci Technol 1994;A12:1229.
[5] Stewart RA, Vitello P, Graves DB. J Vac Sci Technol 1995;B12:478.
[6] Kushner MJ, Collison WZ,Grapperhaus MJ, Holland JP, Barnes MS. J Appl Phys 1996;80:1337.
[7] Passchier JDP, Goedheer WJ. J Appl Phys 1993;74:3744.
[8] Economou DJ, Feldsien J, Wise RS. In: Kortshagen U, Tsendin LD, editors. Electron Kinetics and Applications. New York: Plenum, 1998.
[9] Aydil ES, Economou DJ. J Electrochem Soc 1993;140:1471.
[10] Beale D, Siu S, Patrick R. J Vac Sci Technol 1998;B16:1059.
[11] Bukowski JD, Graves DB, Vitello P. J Appl Phys 1996;80:2614.
[12] Ventzek PLG, Grapperhaus M, Kushner MJ. J Vac Sci Technol 1994;B12:3118.
[13] Meyyappan M, Govindan TR. J Appl Phys 1995;78:6432.
[14] Bose D, Govindan TR, Meyyappan M. J Electrochem Soc 1999;146:2705.
[15] Wise R, Lymberopoulos D, Economou DJ. Appl Phys Lett 1996;68:2499.
[16] Economou DJ, Panagopoulos TL, Meyyappan M. Micro 1998;16(7):101.
[17] Gorbatkin SM, Berry LA, Roberto JB. J Vac Sci Technol 1990;A8:2893.
[18] Yasaka Y, Fukuyama A, Hatta A, Itatani R. J Appl Phys 1992;72:2652.
[19] Koh WH, Choi NH, Choi DI, Oh YH. J Appl Phys 1993;73:4205.
[20] Williamson MC, Lichtenberg AJ, Lieberman MA. J Appl Phys 1992;72:3924.
[21] Hussein MA, Emmert GA, Hershkowitz N, Woods RC. J Appl Phys 1992;72:1720.
[22] Weng Y, Kushner MJ. J Appl Phys 1992;72:33.
[23] Lymberopoulos DP, Economou DJ. IEEE Trans Plasma Sci 1995;23:573.
[24] Lymberopoulos DP, Economou DJ. J Appl Phys 1993;73:3668.
[25] Hughes TJR. The Finite Element Method. Prentice-Hall, 1987.
[26] Reddy JN. Int J Num Methods in Fluids 1982;2:151.
[27] Sani RL, Gresho PM, Lee RL, Griffiths DF. Int J Num Methods in Fluids 1981;1:17.
[28] Hopwood J, Asmussen J. Appl Phys Lett 1991;58:2473.
[29] Tsu DV, Young RT, Ovshinsky SR, Klepper CC, Berry LA. J Vac Sci Technol 1995;A13:935.
[30] King G, Sze FC, Mak P, Grotjohn TA, Asmussen J. J Vac Sci Technol 1992;A10:1265.
[31] Wise RS, Lymberopoulos, Economou DJ. In: Mathad GS, Meyyappan M, Hess DW, editors. Proceedings of the 11th Plasma Processing Symposium [special issue]. The Electrochemical Society 1996;PV-96-12:11.